PAPER

Scalable synthesis of a sulfur nanosponge cathode for a lithium–sulfur battery with improved cyclability†

Junjie Niu, Akihiro Kushima, Mingda Li, Ziqiang Wang, Wenbin Li, Chao Wang and Ju Li*

Although lithium–sulfur batteries exhibit a high initial capacity, production costs and lack of cyclability are major limitations. Here we report a liquid-based, low-cost and reliable synthesis method of a lithium–sulfur composite cathode with improved cyclability. An open network of Conductive Carbon Black nanoparticles (Cnet) is infused with a sulfur network (Snet) to form sponge-like networks (Cnet + Snet). Initially, Snet is open to the outside, allowing liquid electrolyte to infiltrate and impart Snet Li$^+$ conductivity. During lithiation, Cnet could accommodate the volume expansion of Snet largely without losing electrical contact. During delithiation, the carbon nanoparticles would preferably flocculate on the outer surface due to polysulfide dissolution and depletion of sulfur, to form a passivation layer that still allows Li$^+$ exchange, but prevents more polysulfides from escaping, thus slowing the leaching of polysulfides into the bulk electrolyte liquid. The plausibility of a carbonaceous passivation layer was checked using an extra carbon deposition layer to achieve an improved performance of ~400 mA h g^{-1} after 250 cycles under a high rate 2.0 C. A 763 mA h g^{-1} discharge specific capacity of this sulfur nanosponge cathode (abbreviated as "SULFUN") was obtained after 100 cycles under a rate of 0.2 C. Discharge capacities of 520 mA h g^{-1} and 290 mA h g^{-1} were attained after 300 and 500 cycles, respectively, making this cathode material attractive for rechargeable battery applications.

The surging demand for rechargeable batteries in portable electronics and electric vehicles has stimulated extensive studies on various lithium-based electrode materials.[1,2] Sulfur is nontoxic and earth-abundant,[3,4] it hosts two lithium ions non-topotactically, and exhibits a theoretical capacity of 1675 mA h g^{-1}, almost 10 times that of LiCoO$_2$. In terms of the gravimetric energy density, at 2.1 V *versus* Li/Li$^+$, it is still 5 times that of LiCoO$_2$. However, sulfur and its insoluble Li$_2$S$_2$ and Li$_2$S forms are poor electronic conductors. This necessitates the coupling of a certain amount of excellent electron conductors like carbon. Sulfur also does not conduct Li$^+$ ions very well, so intimate contact of the liquid electrolyte with sulfur can be used to enhance the effective Li$^+$ conductivity in the electrode. This is a double-edged sword, however. Researchers have found that lithium–sulfur batteries show initially exceedingly high capacity,[5] but the capacity suffers rapid decay in cycling due to dissolution of soluble lithium polysulfides, Li$_2$S$_X$ ($4 \leq X \leq 8$), into the bulk liquid electrolyte, and/or volume expansion induced mechanical failures and a degrading electronic

conductivity.[6] A conventional sulfur cathode loses 96% of its active sulfur over just ~30 cycles. To retard this loss, strategies[3,4] modifying the electrolyte,[7–11] electrode[12,13] and operating voltage[14] have been proposed. Suo *et al.* used a 'Solvent-in-Salt' electrolyte with ultrahigh salt concentration to achieve a high-energy rechargeable battery.[15,16] A strategy of inhibiting undesirable polysulfide dissolution reactions *via* modifying the charging condition was recently developed by Su *et al.*[14] that led to an ultra-long cycle life (>500 cycles). Additives like graphene,[17,18] mesoporous carbon,[5,19] and conductive polymers[20–24] were exploited to facilitate efficient electron conduction. And by encapsulating sulfur in TiO$_2$ nanoshells with pre-existing voids, the ~80% volume expansion of sulfur in lithiation can be accommodated, so the battery could run over 1000 cycles.[12] While recent progress demonstrated promising enhancements in the performance,[25] improving the cyclability and sulfur utilization through a cost-effective, simple and scalable synthesis is still in demand.

Here we exploit commercially available Conductive Carbon Blacks (such as Super P®) using a facile wet-chemistry method to synthesize a sulfur–carbon nanosponge, whose evolving microstructure in lithiation/delithiation helps to delay the loss of active sulfur and enhance the cyclability. Our strategy is to use cheap carbon black as the base matrix to construct a sulfur-

Department of Nuclear Science and Engineering and Department of Materials Science and Engineering, Massachusetts Institute of Technology, Cambridge, Massachusetts 02139, USA. E-mail: liju@mit.edu

† Electronic supplementary information (ESI) available. See DOI: 10.1039/c4ta04759a

covering-carbon sponge, instead of the traditional carbon-wrapping-sulfur geometry.[12,17] This may sound counter-intuitive, since sulfur is the phase one wants to protect from leaching, so in most nanostructuring strategies people tend to isolate sulfur from the liquid electrolyte by completely encapsulating it. Here this is not done.

In order to construct a well-blended matrix, a three-step process was developed: (1) Conductive Carbon Blacks such as Super P® was first functionalized using hydrochloric acid, as shown in Fig. 1a. Carbon nanoparticles of ∼70 nm in diameter adhere to each other, forming a percolating electrical network (Cnet, Fig. 1a); (2) the as-grown small sulfur particles surrounded by surfactants were dispersed on the matrix using an *in situ* redox reaction under ultrasonic agitation or mechanical stirring (Fig. 1b and c); the ultrasonic agitation will open carbon particle agglomerations, enabling the *in situ* formation of small sulfur–carbon clusters (2–4 μm), as shown in Fig. 2c and d. For comparison, a well-mixed S–C composite *via* mortar-milling without sonication displays separate, flat sulfur flakes with much larger sizes of 40–60 μm (Fig. 2b). (3) During heating at an annealing temperature of 150 °C or 200 °C, the distributed sulfur melted and deeply infiltrated the framework to form a sulfur-covering-carbon configuration (Fig. 1d, 2e and f). Since the melting temperature of sulfur is 115.2 °C, annealing would cause the sulfur particle to melt, wet and spread across the carbon surface, forming another percolating network (Snet). Cnet and Snet interpenetrate each other and are in intimate contact, forming a nanostructured sponge which we call SUL-FUN (see the Experimental details section). During lithiation/delithiation, the sponge-like structure of Cnet has the ability to breathe to accommodate the ∼80% volume expansion of the Snet without losing electrical contact, according to the porosity evaluation. SULFUN has a different initial topology (Cnet + Snet, with both initially open to the outside) from the carbon-wrapping-sulfur approach[12,17] where one aims to completely encapsulate and isolate the sulfur.

The battery performance of SULFUN was measured *via* coin cells, which were assembled inside a glove box. SULFUN was used as the cathode while a Li foil served as the anode, in an electrolyte of 1.0 M lithium bis-trifluoromethanesulfonylimide (LiTFSI) in 1,3-dioxolane (DOL) and 1,2-dimethoxyethane (DME) (DOL : DME = 1 : 1 in volume). As Snet is initially open to the outside, the LiTFSI + DOL + DME liquid electrolyte wets and infiltrates Snet in the initial lithiation, dissolving some sulfur and forming some soluble lithium polysulfides. The "wet" Snet then has some significant Li$^+$ conductivity, that percolates within Cnet.

Fig. 3a depicts an initial discharge specific capacity of ∼1100 mA h g^{-1} at a rate of 0.2 C (C rate is calculated based on the theoretical capacity 1675 mA h g^{-1} of sulfur). Two main plateaus appear in the discharging window of 2.5 to 1.5 V (Fig. 3a). The first plateau (I) centering at ∼2.3 V corresponds to the sequential reduction of sulfur (S_8) to high-order polysulfides Li_2S_X ($4 \leq X \leq 8$). During the complex reactions, a series of soluble lithium polysulfides are generated.[14] As illustrated in the discharge curve, this plateau is quite short, which only presents a minor capacity of ∼165 mA h g^{-1} (about 15% of the overall 1100 mA h g^{-1}). Then there is a short transition (II), which contributes a small portion, ∼146 mA h g^{-1} (∼13%), as well. Such a fast reaction mitigates the loss of sulfur by way of soluble polysulfides (the "shuttling effect"). A big plateau (III) is located at ∼2.06 V, which is attributed to the continuous conversion of Li_2S_X ($4 \leq X \leq 8$) to low order Li_2S_2 and Li_2S. In this last step, sulfur is reduced to the final state of insoluble Li_2S.[26] The dominance of this reaction is evidenced by the long plateau which constitutes a major portion (∼64%) of the total capacity. Although the insoluble sulfides can increase the volume and the electrical resistance,[26] plenty of interlinked carbon nanoparticles maintain good electron conduction paths to ensure uninterrupted lithiation/delithiation. In other words, Cnet is mechanically robust enough and has a nano-pore-like configuration (specific surface area: >70 m^2 g^{-1}) with flexibility that it can accommodate the ∼80% volume change of Snet by unfolding, while maintaining good electrical conductivity and contact with Snet. Otherwise the cycling performance would degrade very rapidly, which was indeed historically the case.[12]

Shown in Fig. 3b (red) is the cycling capability of the SULFUN cathode annealed at 200 °C. With a charging–discharging rate of 0.2 C, a specific discharge capacity as high as ∼763 mA h g^{-1} was retained after running 100 cycles. After 300 cycles, a ∼520 mA h g^{-1} capacity was still retained, which implies less than 0.2% decay for each cycle (Fig. 3b). The capacity was maintained at a high level of ∼290 mA h g^{-1} even at the 500th cycle. A long-cyclability coin cell made of the same matrix is shown in Fig. S1,† demonstrating reproducibility. Because of the multi-step procedure during material synthesis and battery assembly, a variation in performance inevitably exists. The 150 °C annealed sample displays a better cycling behavior, as evidenced in Fig. 3c. After being subjected to extremely long cycling such as 1500 cycles, the discharge capacity of one cell is still as high as 158 mA h g^{-1} (Fig. 3c). It is noted that after running 1100 cycles, the capacity shows almost no drop (Fig. 3c inset). A comparison of battery performance using the current method with literature is shown in Table S1.†[15,27–31]

For microstructural comparison, coin cells made of commercial pure sulfur and mortar-milled S–C mixture cathodes were also tested, as shown in Fig. 3b and S1.† For the pure sulfur, the capacity drastically decreased from ∼856 mA h g^{-1} to
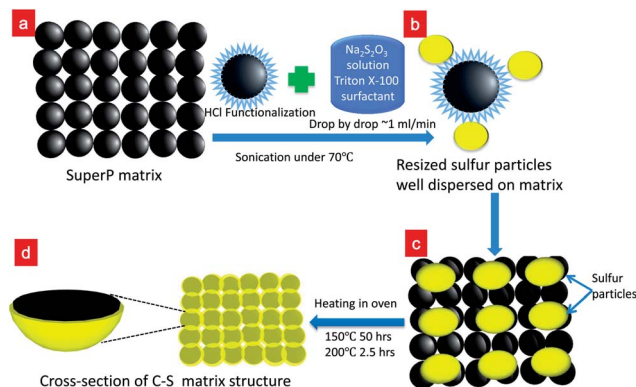

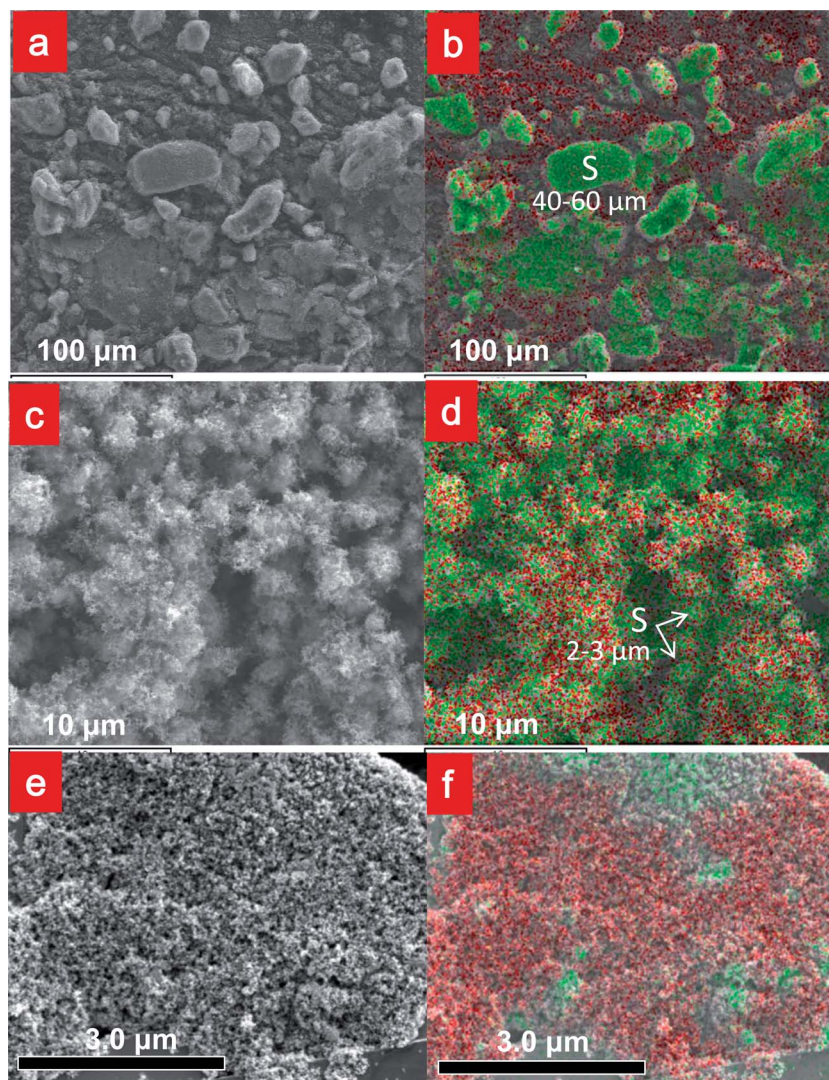**Fig. 1** Schematic of the *in situ* synthesis of SULFUN matrix.

Fig. 2 SEM images and the corresponding energy-dispersive X-ray spectroscopy (EDS) mappings. SEM morphology of the milled S–C mixture (a). SEM morphologies of the SULFUN matrix before (c) and after (e) annealing at 200 °C for 2.5 hours. (b), (d) and (f) Sulfur and carbon mapping of the areas shown in (a), (c) and (e), respectively.

less than 200 mA h g^{-1} after only 15 cycles. The battery almost died after 29 cycles. As for the mortar-milled S–C mixture, the capacity dropped to less than 300 mA h g^{-1} after 100 cycles and almost down to zero at the 200th cycle (Fig. 3b, blue). The two plateaus from the charge–discharge voltage profile almost disappeared after 200 cycles (Fig. S3†) while they were still observed even after 1500 cycles in SULFUN (Fig. S2†). We further found that in the coin cell assembly of the SULFUN cathode, by adding a trace of conductive polymer polypyrrole (PPy) to the SULFUN/binder/Super P® slurry, this acts as a network to restrain the dissolution of intermediate products. It will not impair Li$^+$/e$^-$ transport due to the relatively high electric conductivity (0.005 S cm^{-1}) of PPy. The ability to trap both polysulfides and the possibly detached sulfur particles without raising resistance can further deter the fast fading of capacity.

The morphology of sulfur was characterized by electron microscopy. As shown in Fig. S4a,† the as-fabricated sulfur without a carbon host shows sizes ranging 5–10 μm. The commercial sulfur after mortar-milling displays sizes ranging 40–60 μm (Fig. 2a and b). However, during the SULFUN fabrication step (2), the size of sulfur particles dispersed on the carbon matrix surface becomes smaller (Fig. 2c, d and S5d, e†). It reveals sulfur particles with sizes of 2–4 μm, which is about 50% less than the free-standing sulfur in Fig. S4a† and much smaller than the commercial pure (Fig. 4a) and mortar-milled (Fig. 2a and b) sulfur. The sulfur was dispersed rather uniformly on the carbon surface, as illustrated from the energy-dispersive X-ray spectroscopy (EDS) mapping in Fig. 2d and S5d.† In contrast to the separate sulfur particles after milling (Fig. 2a and b), the semi-closed ball-like S–C cluster with smaller sizes ensures a sufficient contact, leading to a high ion/electron conductivity (Fig. 2c and d). In order to further reduce the microstructural length scale and form a compact nanoscale S–C network, the sulfur was subsequently melted during the SUL-FUN fabrication step (3) at 150 °C or 200 °C, respectively. Under this temperature, like water filtrating a sponge, the fluidic
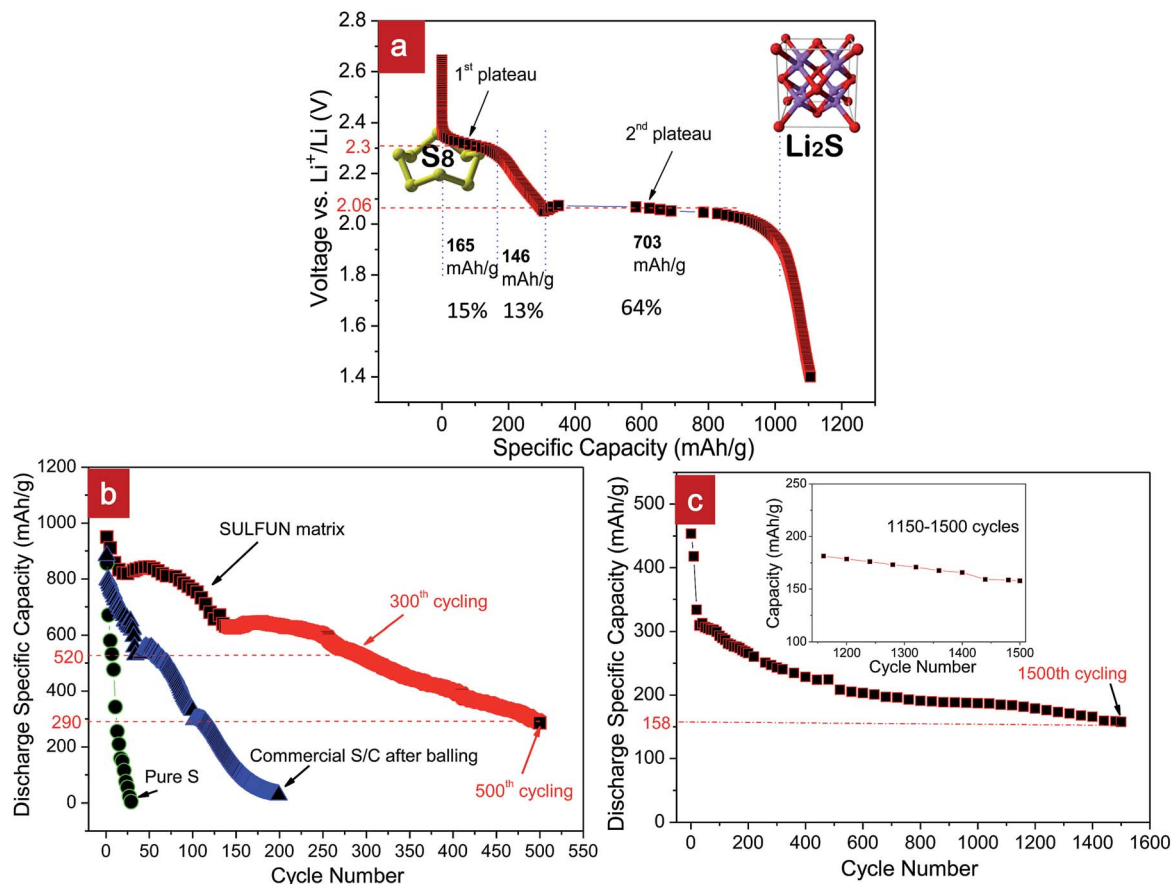
Fig. 3 Discharge voltage profiles of SULFUN matrix. Discharge voltage profile of the matrix treated at 200 °C with 2.5 hours at a rate of 0.2 C (a). Cycling performance of commercial pure sulfur (green), mortar milled S–C mixture (blue), and SULFUN matrix (red) treated under 200 °C for 2.5 hours (b) and 150 °C for 50 hours (c) at a rate of 0.2 C.

sulfur permeated inside the sponge (Fig. 1d). As displayed in Fig. 2e, f and S4b, c,† the sulfur can almost not be isolated from Cnet any more. A TEM image of the 200 °C treated sample also exhibits a uniform composition (Fig. S5f†). Elemental mapping of a local area clearly shows a proportional distribution of sulfur and carbon (Fig. 2f and S5a–c†). These data imply that Snet has been interfused with nanostructured Cnet, improving the adhesion between sulfur and carbon, providing a fast pathway for ion/electron transport. According to the estimated volume of the matrix, the gravimetric loading of sulfur is about 70 wt%. Quantitative thermal-gravimetric analysis (TGA) reveals the actual loading of sulfur in SULFUN was 62–65 wt% (Fig. S6†).

The initial size of sulfur plays a critical role on the imbibition process and the later cyclability. To obtain a homogenous cathode, well-dispersed sulfur particles with a small size are significant. In the present modifications, Carbon Blacks first underwent acid treatment in hydrochloride to create hydroxyl/ carboxyl functional groups. In parallel, the added surfactant groups encapsulated the fresh sulfur particles to prevent Ots-wald ripening. They also made the sulfur particles more effi-ciently distributed over the framework. Then, a very important step is the extremely slow redox process. The sodium thiosulfate solution was added dropwise to the functionalized carbon solution with vigorous agitation. In this situation, sulfur, with a

reduced size, uniformly spreads over a wide area of the carbon surface, before it melts and spreads further by annealing at 150 °C for 50 hours or 200 °C for 2.5 hours (Fig. 2c and d). However, the commercially ground and pure sulfur possess much larger sizes of 40–60 μm (Fig. 2a, b and 4a, b).

Next, we investigated the morphological evolution of the electrode surface during lithiation/delithiation. As can be seen from Fig. 4a, the surface of the original commercial sulfur is quite smooth. A clear boundary between sulfur and other materials like carbon and binder is observed *via* elemental mapping (Fig. 4b). However after only two cycles, several holes, with sizes of 2–4 μm, were observed on the sulfur particles, which by then were already severely deformed and shrunk, indicating a rapid loss of the active sulfur (Fig. 4c, d and S7†). The sulfur particles were dramatically deformed and broke into smaller particles which were dispersed across the surface inhomogeneously (Fig. S7†). In contrast, the surface of the SULFUN electrode is still smooth after cycling, as shown in Fig. 4e. The elemental mapping of sulfur indicates a homoge-neous distribution (Fig. 4f). From analysis of the cross-section of the pure sulfur electrode, O and F, which can only be precipitated out from the electrolyte, was found to be dispersed across the whole electrode film (∼40 μm, Fig. 5a), indicating deep invasion of the liquid electrolyte and corrosion of the
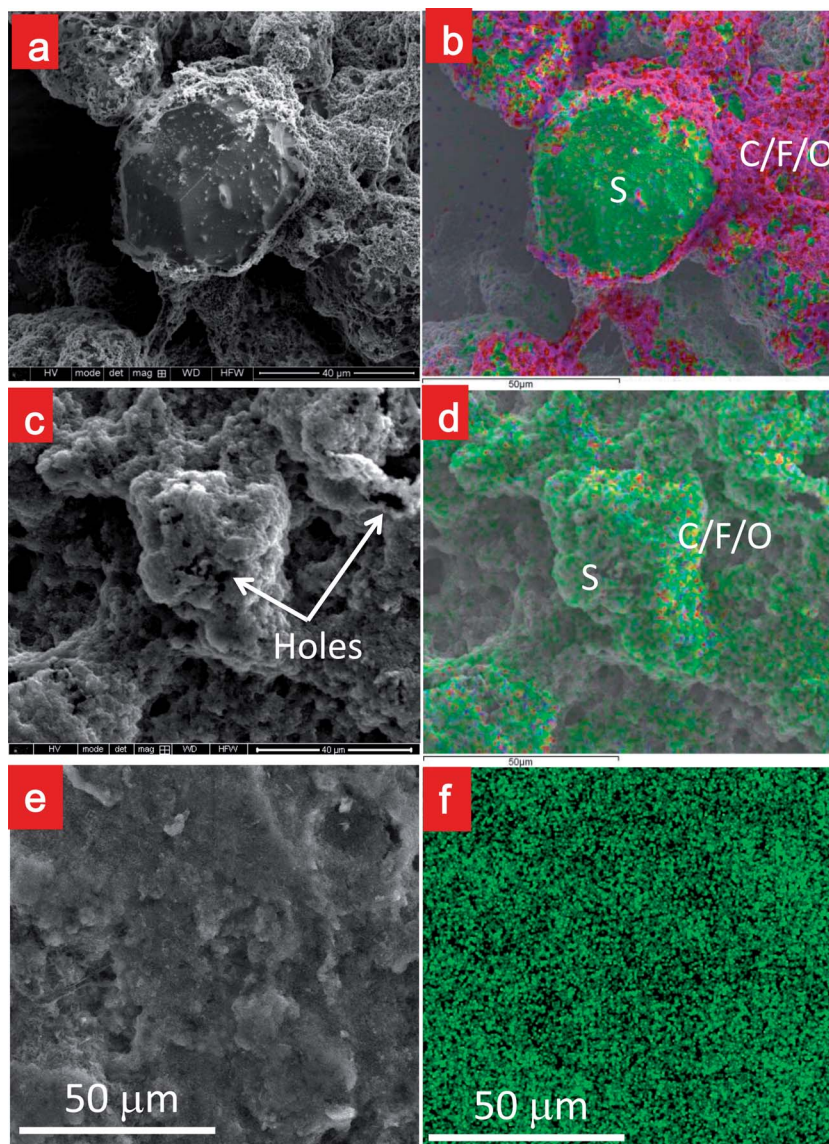
Fig. 4 Morphology evolution of commercial sulfur particle and SULFUN during the charge−discharge. SEM morphologies of the commercial sulfur mixture with Super-P® and binder before (a) and after (c) two rounds of cycling. (b) and (d) EDS element mappings of the area shown in (a) and (c), respectively. (e) SEM morphology of the electrode made of the SULFUN annealed at 200 °C for 2.5 hours after two cycles. (f) The corresponding sulfur element mapping from (e).

sulfur. However, the O and F elements were highly concentrated on the top surface (1–2 μm) of the SULFUN electrode and scarcely found inside (Fig. 5b and S8†), indicating liquid electrolyte invasion and the sulfur corrosion were suppressed. The corrosion reaction is believed to be heterogeneous and anisotropic, as schematically illustrated in Fig. 6a and S9a.† Some locations will be more heavily corroded and consequently will generate holes/cracks, causing the whole particle to split (Fig. 6a). The electrode surface composed of pure or milled sulfur displays a larger solid–liquid interface, $S_{contact}$, to the liquid electrolyte but with a smaller volume of sulfur V_s (Fig. 6b and S9a†). In this case, the liquid electrolyte can easily permeate into the electrode (Fig. 5a), which also creates a path to carry away the soluble polysulfides. However, the compactly nanostructured SULFUN exposes only a very small area of naked

sulfur to the liquid electrolyte (Fig. 6c and S9b†) limiting the sulfur dissolution, even when the intermediate lithium polysulfides are formed inside. Here a possible mechanism is suggested. Because Snet is initially open to the outside, the LiTFSI + DOL + DME liquid electrolyte wets and infiltrates Snet in the initial lithiation, dissolving some sulfur and forming some soluble lithium polysulfides. "Wet" Snet then has some significant Li$^+$ conductivity, that percolates within Cnet. However, once the embedded sulfur on the top is "blown away", the carbon nanoparticles remaining (tens to hundreds of nanometers, as shown in Fig. 5b and S8†) will possibly concentrate to form a rather dense carbon-rich layer as a passivation layer against corrosion, which serves like a sieve to selectively block larger molecules such as the electrolyte and polysulfide while allowing small Li$^+$/e$^-$ to pass through (Fig. 6c and S9†).
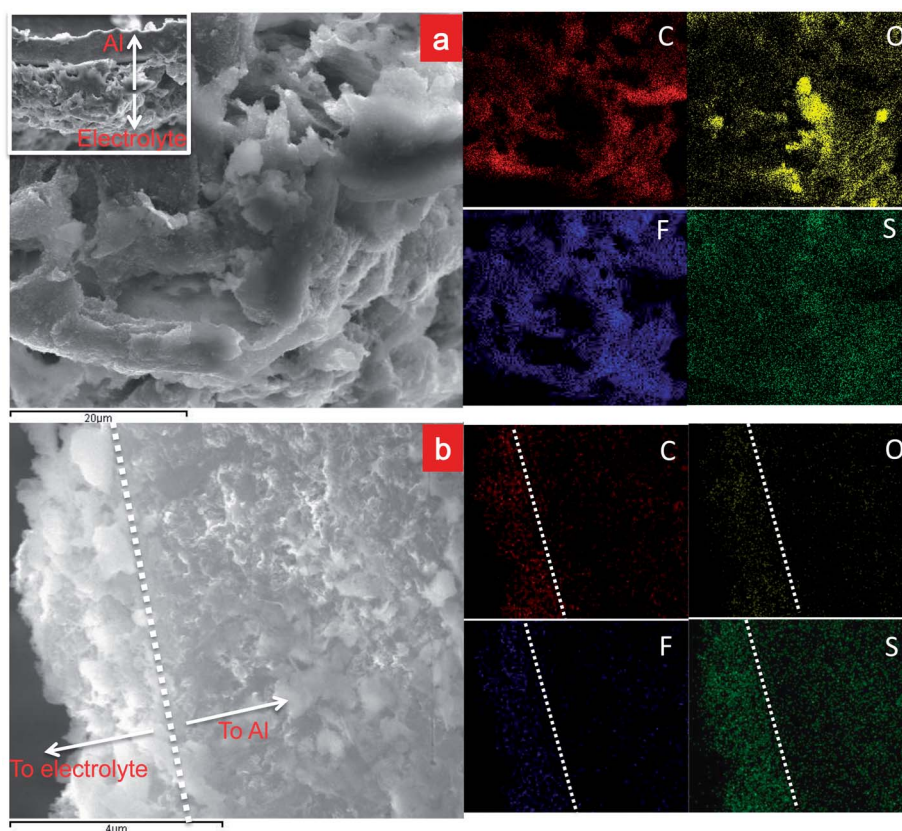
Paper

Fig. 5 Cross-section diagnosis of the electrode after two charge–discharge cycles. SEM images and the corresponding EDS element mappings of the cross-section of the electrode made of commercial sulfur (a) and SULFUN (b). The mapping data indicate that electrolyte invasion was suppressed by the SULFUN surface relative to the commercial sulfur surface.
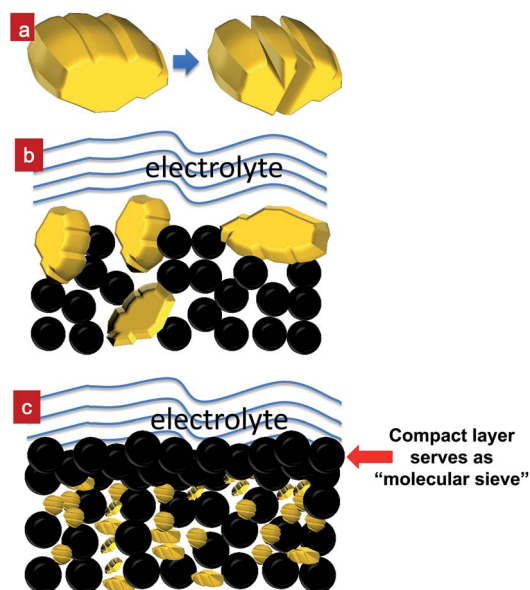

Fig. 6 Schematic of the reaction mechanism during the charging–discharging. (a) The sulfur particle generates holes/cracks due to the anisotropic reaction. The commercial sulfur particle shows a much larger $S_{contact}/V_s$ ratio (b) compared to the compact SULFUN matrix (c), which greatly delays the loss of sulfur.

To verify that the carbon layer has the effect of preventing sulfur corrosion, an additional carbon layer with tens of μms thickness was coated on the SULFUN surface. Fig. 7 shows the cycling performance and coulombic efficiency of the modified SULFUN battery at different charge–discharge rates. As can be seen from Fig. 7a, an initial >1300 mA h g^{-1} capacity was achieved and then was maintained at a value of ~1100 mA h g^{-1} until 60 cycles, with the coulombic efficiency >98%. Under the 10 times faster charging–discharging (2.0 C), a special discharge capacity of ~400 mA h g^{-1} was still attained after 250 cycles (Fig. 7b). This high rate capability indicates the extra carbon can act as a passivation layer to reduce the "shuttling effect", as the *in situ* formed carbon-rich passivation layer on SULFUN surface, leading to a long battery life.

To better understand the selective permeation effect, we calculate the size dependence of the molecule/ion on the solubility and diffusion coefficient inside the Super P®. The mass transport flux is proportional to the product of the solubility and the diffusion coefficient in carbon black, as[32–34]

$$J \sim \frac{k_B T}{6\pi M^{1/2} a} \exp\left(-\frac{Q}{k_B T}\right), \quad (1)$$

where k_B is the Boltzmann constant, T is temperature, M and a are the mass and the average radius of the molecule/particle, respectively. Q is the effective activation energy, combining both

This journal is © The Royal Society of Chemistry 2014

J. Mater. Chem. A, 2014, **2**, 19788–19796 | **19793**
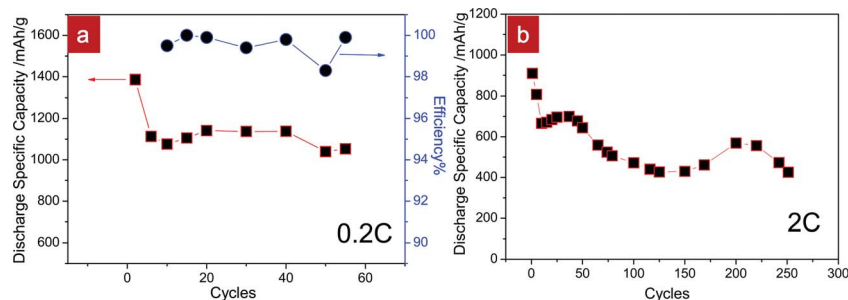
Fig. 7 Cycling performance of modified SULFUN coin cells at the different charge–discharge rates. The cyclability of batteries made of SULFUN coated with an additional carbon layer at 0.2 C with coulombic efficiency (a) and at 2.0 C (b), respectively. 0.1 M LiNO$_3$ was added into the electrolyte solution.

insertion energy and migration energy barrier. When a molecule/ion in the liquid electrolyte is inserted into and diffuses inside the passivation layer, both interfacial and elastic energies contribute to Q:[35]

$$Q \approx F_{\text{surface}} + F_{\text{elastic}} = 4\pi a^2 \gamma + \frac{24\pi a^3 \mu K \varepsilon^2}{3K + 4\mu}, \qquad (2)$$

where γ is the interfacial energy, K, μ and ε are the bulk modulus, shear modulus and dilatational misfit strain, respectively. For small particles such as a single lithium ion, molecular sulfur/polysulfide ion, or even electrolyte, $F_{\text{surface}} \gg F_{\text{elastic}}$, and eqn (2) becomes $Q \approx S\gamma$. Here, S is the surface area. The average surface energy of Super P® is $\sim$100 mJ m^{-2} (ref. 36 and 37) and the surface area of a Li ion, small sulfur molecules S$_4$ and S$_8$ can be estimated using lithium ion radius of 1.34 Å and the bond length values of various small sulfur molecules.[38] Thus, we obtain from eqn (1) and (2) the ratio of permeation fluxes $J(X)$ (X = Li, S$_4$, S$_8$) as $J(\text{Li}) : J(\text{S}_4) : J(\text{S}_8) = 1 : 10^{-3} : 10^{-8}$, showing the permeation of the S$_8$ cluster is eight orders of magnitude slower than Li. The upshot of the above rough estimation is that a pure carbon layer (blocking the invasion of the liquid electrolyte into Snet) can selectively allow Li$^+$/e$^-$ to easily enter, but prevents the larger polysulfides Li$_2$S$_X$ ($4 \le X \le 8$) from coming in or out, thus slowing down the shuttling effect[6] and acting as a passivating molecular sieve. Also, the fine-meshed Cnet will probably restrain and block much smaller sulfur particles from breaking off Snet mechanically and convecting into the liquid. In other words, the SULFUN nanocomposite can better facilitate stress relaxation and enhance flaw tolerance, which is maybe a generic behavior of nano-scale electrode materials.

In conclusion, the *in situ* synthesized sulfur–carbon nanosponge using Conductive Carbon Blacks as a host greatly slowed down the loss of sulfur, hereby displaying a better cycling performance while maintaining a high capacity. The suggested passivation layer or extra carbon layers can prevent the decay of capacity by limiting the transport of the larger polysulfides Li$_2$S$_X$ ($4 \le X \le 8$) without slowing down Li$^+$/e$^-$. This "defense-in-depth" strategy is distinct from the complete encapsulation or the "defense-in-perimeter" strategy most researchers have employed. Our improved coin-cell scale performance indicates that the polysulfides shuttling effect is ameliorable through nanostructural design and engineering. The high capacity, long cyclability, cheap raw materials and simple preparation make the SULFUN cathode material a potential candidate on the scale of industrial production.

Experimental details

In situ synthesis of S–C sponge matrix

Details of the *in situ* synthesis of sulfur–carbon sponge matrix are as follows. 70 wt% (according to the approximate loading in the final S–C matrix) Conductive Carbon Blacks (Super C65, Timical) were first treated in a solution mixed with 20 ml hydrochloric acid (1 N volumetric solution, Avantor Performance Materials, Inc.) under stirring on a hot plate (Super-Nuova, Thermo Scientific) for 2 hours at 70 °C. Then 100 ml deionized water was added. Meanwhile, sodium thiosulfate (anhydrous, 99%, Alfa Aesar) was dissolved in 150 ml deionized water with surfactant Triton X-100 (1% in deionized water, Alfa Aesar).[17] Then, the sodium thiosulfate solution was added to the Conductive Carbon Black solution with a dropping speed of $\sim$1 ml min^{-1} under ultrasonic agitation (Symphony, VWR Ultrasonic Cleaner) at a constant temperature of 70 °C. The reacted sample was centrifuged (IEC HN-SII Centrifuge, Damon/IEC Division) and dried at 60 °C in an oven (Symphony, VWR). Finally, the dried mixture was annealed at temperatures of 150 °C for 50 hours ("low-temperature") or 200 °C for 2.5 hours ("high-temperature") in air, respectively. The collected samples were stored for coin cell assembly and battery performance tests.

For comparison, 80 wt% commercial sulfur (sulfur powder, 99.5%, Alfa Aesar), 10 wt% Super P® and 10 wt% binder were uniformly milled for 30 minutes in a mortar. After the milling, the mixture was applied to make a slurry on Al foil and then the final coin cell was assembled using the same protocol.

Characterization of morphology, chemical composition, and structure

SEM. The surface morphologies were checked by scanning electron microscopy using an FEI/Philips XL30 FEG Environmental Scanning Electron Microscope (ESEM), FEI/Philips Helios Nanolab 600 Dual Beam Focused Ion Beam Milling

19794 | *J. Mater. Chem. A*, 2014, **2**, 19788–19796

This journal is © The Royal Society of Chemistry 2014

System, and JEOL 6320 Field-Emission High-Resolution SEM at 5–10 kV incident energy. The carbon–sulfur elemental mapping was obtained through energy-dispersive spectroscopy micro-analysis using an INCA EDS detector at 20 kV acceleration voltage.

TEM. The as-grown sulfur and S–C sponge treated at different annealing temperatures were characterized by transmission electron microscopy (TEM) using a JEOL JEM-2010F at an accelerating voltage of 200 kV. The TEM sample was dispersed on a lacy carbon film supported on a copper grid to acquire the images. In order to reduce electron-beam damage, a low magnification with a weak beam intensity was applied when the images were captured.

TGA. Thermal gravimetric analysis (TGA, SEIKO SSC/5200 TG/DTA220 thermal analysis station) and differential scanning calorimetry curves were recorded in argon as the working gas. The temperature program was set to be isothermal at 50 °C for 10 min and heated up to 650 °C with a heating rate of 10 °C min^{-1}.

Assembling the coin cell and testing battery performance

The battery behavior of the synthesized material was performed *via* a coin cell. Typically, a CR2032 coin cell (MTI) with a lithium foil as the counter/reference electrode was assembled in an argon-filled glove box (LABmaster SP, MBraun) where both O_2 and H_2O concentrations were lower than 0.1 ppm. The Celgard 2400 was used as the separator. For the liquid electrolyte, we used the typical 1.0 M lithium bis-trifluoromethanesulfonylimide in 1,3-dioxolane and 1,2-dimethoxyethane (volume ratio 1 : 1, Novolyte). All of the battery performances were tested without additives except the rate data shown in Fig. 7. A hydraulic crimping machine (MSK-110, MTI) was employed to close the cell. To make a slurry, the active material of sulfur–Super P® sponge, or pure sulfur synthesized using the same method but without carbon, or milled sulfur–carbon mixture was blended with 10 wt% Super C65 (Timical), 10 wt% poly(vinylidene fluoride) binder, and a small amount of polypyrrole solution (polypyrrole doped, 5 wt% dispersion in H_2O, conductivity of dried cast film: >0.0005 S cm^{-1}, Sigma-Aldrich) dissolved in *N*-methylpyrrolidone (MTI). The sulfur loading was designed to be 1.0 mg cm^{-2} for 150 °C sample and 2.0 mg cm^{-2} for 200 °C sample, respectively. The mixture was sonicated until a homogeneous slurry was formed. Then the slurry was coated onto an aluminum foil current collector. After drying for 2 hours at 90 °C in an oven, the sample was cut to serve as an cathode.

For the high-rate charge–discharge test, an additional layer composed of the carbon/binder was coated on the top of the SULFUN dried slurry. In a typical experiment, the melted sulfur–carbon mixture with 10 wt% Super P® and 10 wt% poly(vinylidene fluoride) binder was first coated on the aluminum foil, as described above. After the first slurry was almost dried, the secondary slurry composed of Super P® (80 wt%) and binder (20 wt%) with a loading of ~2.0 mg cm^{-2} was coated on the surface. Then the sample was dried overnight at 65 °C in an oven for battery assembling.

The packed coin cell was galvanostatically charged–discharged in a fixed voltage window between 1.4 and 2.5/2.8 V on a 12-channel Arbin Instruments BT2000 battery tester at room temperature. The cycling capability was recorded at a charging–discharging rate of 0.2 C and 2.0 C, respectively. The discharge specific capacity was calculated based on the actual sulfur loading corrected by the TGA test.

Acknowledgements

References

1 P. G. Bruce, S. A. Freunberger, L. J. Hardwick and J. M. Tarascon, *Nat. Mater.*, 2012, **11**, 19–29.
2 R. Van Noorden, *Nature*, 2013, **498**, 416–417.
3 A. Manthiram, Y. Z. Fu and Y. S. Su, *Acc. Chem. Res.*, 2013, **46**, 1125–1134.
4 Y. X. Yin, S. Xin, Y. G. Guo and L. J. Wan, *Angew. Chem., Int. Ed.*, 2013, **52**, 13186–13200.
5 X. L. Ji, K. T. Lee and L. F. Nazar, *Nat. Mater.*, 2009, **8**, 500–506.
6 Y. V. Mikhaylik and J. R. Akridge, *J. Electrochem. Soc.*, 2004, **151**, A1969–A1976.
7 Z. Lin, Z. C. Liu, W. J. Fu, N. J. Dudney and C. D. Liang, *Angew. Chem., Int. Ed.*, 2013, **52**, 7460–7463.
8 E. Peled, Y. Sternberg, A. Gorenshtein and Y. Lavi, *J. Electrochem. Soc.*, 1989, **136**, 1621–1625.
9 S. E. Cheon, K. S. Ko, J. H. Cho, S. W. Kim, E. Y. Chin and H. T. Kim, *J. Electrochem. Soc.*, 2003, **150**, A800–A805.
10 L. X. Yuan, J. K. Feng, X. P. Ai, Y. L. Cao, S. L. Chen and H. X. Yang, *Electrochem. Commun.*, 2006, **8**, 610–614.
11 J. H. Shin and E. J. Cairns, *J. Power Sources*, 2008, **177**, 537–545.
12 Z. W. Seh, W. Li, J. J. Cha, G. Zheng, Y. Yang, M. T. McDowell, P.-C. Hsu and Y. Cui, *Nat. Commun.*, 2013, **4**, 1331.
13 J. Wang, S. Y. Chew, Z. W. Zhao, S. Ashraf, D. Wexler, J. Chen, S. H. Ng, S. L. Chou and H. K. Liu, *Carbon*, 2008, **46**, 229–235.
14 Y. S. Su, Y. Z. Fu, T. Cochell and A. Manthiram, *Nat. Commun.*, 2013, **4**, 2985.
15 L. M. Suo, Y. S. Hu, H. Li, M. Armand and L. Q. Chen, *Nat. Commun.*, 2013, **4**, 1481.
16 Y. Sun, L. Zhao, H. L. Pan, X. Lu, L. Gu, Y. S. Hu, H. Li, M. Armand, Y. Ikuhara, L. Q. Chen and X. J. Huang, *Nat. Commun.*, 2013, **4**, 1870.
17 H. L. Wang, Y. Yang, Y. Y. Liang, J. T. Robinson, Y. G. Li, A. Jackson, Y. Cui and H. J. Dai, *Nano Lett.*, 2011, **11**, 2644–2647.
18 M. K. Song, Y. G. Zhang and E. J. Cairns, *Nano Lett.*, 2013, **13**, 5891–5899.
19 N. Jayaprakash, J. Shen, S. S. Moganty, A. Corona and L. A. Archer, *Angew. Chem., Int. Ed.*, 2011, **50**, 5904–5908.
20 Y. Z. Fu and A. Manthiram, *RSC Adv.*, 2012, **2**, 5927–5929.

This journal is © The Royal Society of Chemistry 2014

J. Mater. Chem. A, 2014, **2**, 19788–19796 | 19795

21 X. Liang, Y. Liu, Z. Y. Wen, L. Z. Huang, X. Y. Wang and H. Zhang, *J. Power Sources*, 2011, **196**, 6951–6955.

22 H. K. Song and G. T. R. Palmore, *Adv. Mater.*, 2006, **18**, 1764–1768.

23 J. L. Wang, J. Yang, J. Y. Xie and N. X. Xu, *Adv. Mater.*, 2002, **14**, 963–965.

24 Y. Yao, N. Liu, M. T. McDowell, M. Pasta and Y. Cui, *Energy Environ. Sci.*, 2012, **5**, 7927–7930.

25 G. Y. Zheng, Y. Yang, J. J. Cha, S. S. Hong and Y. Cui, *Nano Lett.*, 2011, **11**, 4462–4467.

26 C. Barchasz, F. Molton, C. Duboc, J. C. Lepretre, S. Patoux and F. Alloin, *Anal. Chem.*, 2012, **84**, 3973–3980.

27 J. Schuster, G. He, B. Mandlmeier, T. Yim, K. T. Lee, T. Bein and L. F. Nazar, *Angew. Chem., Int. Ed.*, 2012, **51**, 3591–3595.

28 C. F. Zhang, H. B. Wu, C. Z. Yuan, Z. P. Guo and X. W. Lou, *Angew. Chem., Int. Ed.*, 2012, **51**, 9592–9595.

29 G. Y. Zheng, Q. F. Zhang, J. J. Cha, Y. Yang, W. Y. Li, Z. W. Seh and Y. Cui, *Nano Lett.*, 2013, **13**, 1265–1270.

30 W. Weng, V. G. Pol and K. Amine, *Adv. Mater.*, 2013, **25**, 1608–1615.

31 S. Xin, L. Gu, N. H. Zhao, Y. X. Yin, L. J. Zhou, Y. G. Guo and L. J. Wan, *J. Am. Chem. Soc.*, 2012, **134**, 18510–18513.

32 R. B. Bird, W. E. Stewart and E. N. Lightfoot, *Transport Phenomena*, Wiley, New York, 1960.

33 J. L. Anderson and C. C. Reed, *J. Chem. Phys.*, 1976, **64**, 3240–3250.

34 A. Dondos and H. Benoit, *Polymer*, 1977, **18**, 1161–1162.

35 F. S. Henry Ehrenreich, *Solid State Physics: Advances in Research and Applications*, Elsevier Academic Press, 2004, vol. 59.

36 M. L. GonzalezMartin, B. Janczuk, L. LabajosBroncano and J. M. Bruque, *Langmuir*, 1997, **13**, 5991–5994.

37 J.-B. Donnet, R. C. Bansal and M.-J. Wang, *Carbon black: science and technology*, Dekker, New York, 1993.

38 B. Meyer, *Chem. Rev.*, 1976, **76**, 367–388.

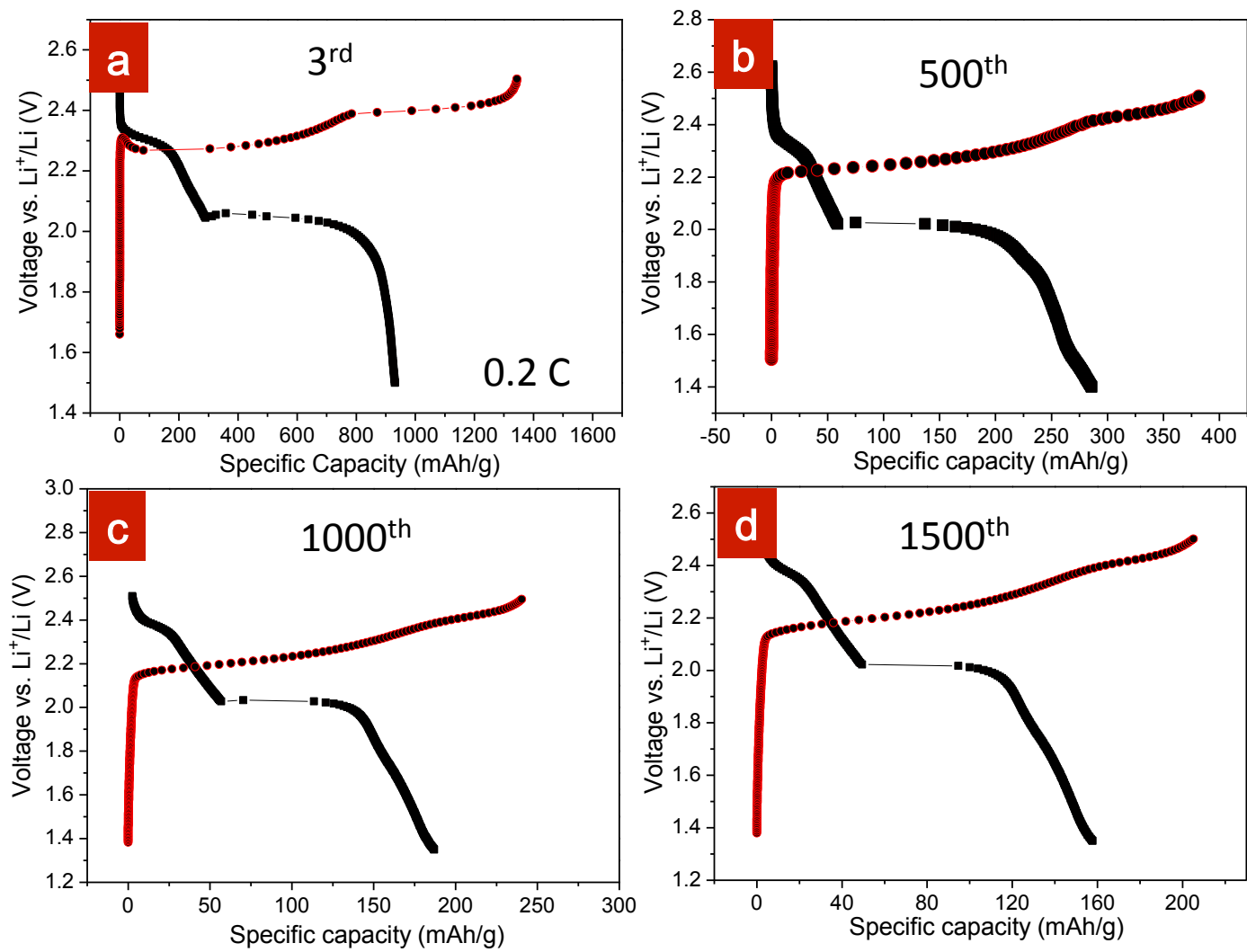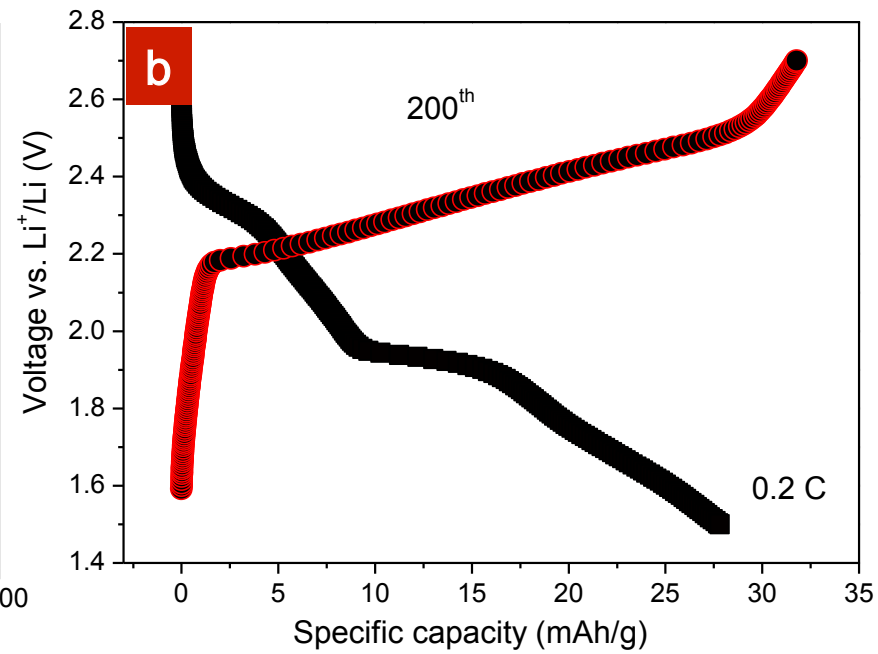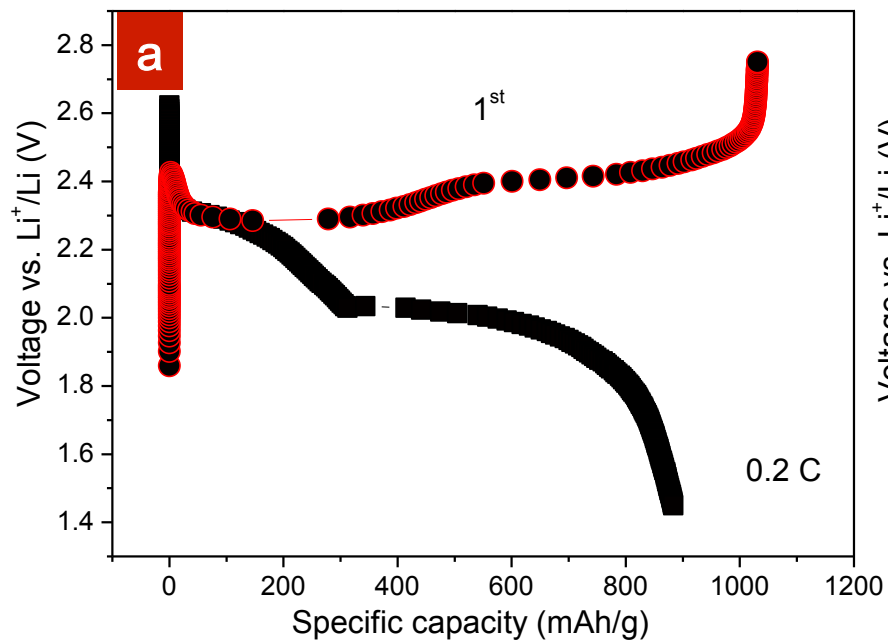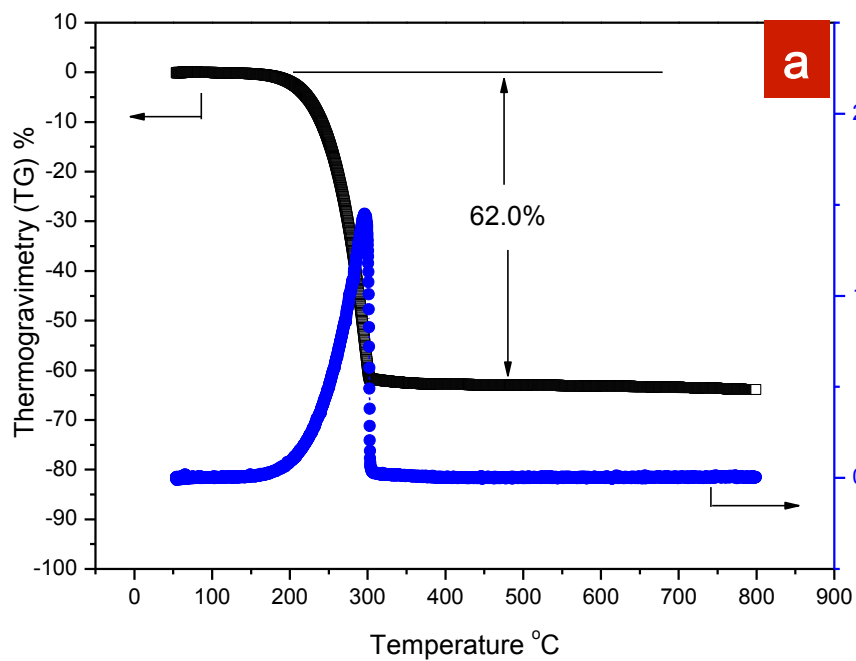| Approach	1st discharge Capacity (mAh/g)	Reversible discharge capacity (mAh/g)	Charge rate (mA/g)	Total cycle number	Degradation rate per cycle	Sulfur Loading	Ref.
SULFUN	1000-1400	520 (300th, 0.2C) 290 (500th, 0.2C) 400 (250th, 2C)	335 (0.2C) 3350 (2C)	>500	0.24% (0.2C) 0.36% (2C)	65 wt% (2mg/cm^2)	Current work
S-TiO$_2$ yolk-shell nanocomposite	1,030	690	836 (C/2)	1,000	0.033%	53 wt % 0.4–0.6 mg/cm^2	12
Solvent-in-salt electrolyte	1,041	770	335 (C/5)	100	0.26%	48 wt %	15
Ordered mesoporous C-S	1,070	700	1675 (1C)	100	0.35%	57 wt %	27
Double-shelled C-S composite	1,020	690	167 (C/10)	100	0.32%	45 wt %	28
Porous hollow C-S composite	1,071	974	836 (C/2)	100	0.09%	65 wt %	19
Hollow CNF-encapsulated S	~1,400	730	836(C/2)	150	0.48%	~1.0 mg / cm^2	25
Amphiphilic surface-modified hollow CNF-S	828	~660	836 (C/2)	300	0.07%	~1.0 mg / cm^2	29
Ultrasound-assisted S-C with fluorinated ether	1,195	836	230	100	0.30%	29 wt %	30
S molecules in a C/CNT matrix	1,670	1,142	167.5 (C/10)	200	0.16%	32 wt %	31
Li-S with interlayers with modified recharge setting	1,483	600 and 1000	335 (C/5)	>300 (600mAh/g) >200 (1000mAh/g)	0.0011% (600mAh/g) 0.0027% (1000mAh/g)	70 wt%	14

Table S1

Fig. S1

Fig. S2

Fig. S3

Fig. S4

a
15um

b C
15 μm

c S
15 μm

d
C
S
15um

e Sulfur particles

f

Fig. S5

Fig. S6

Fig. S7

To electrolyte

C

O

F

S

10μm

10μm

10μm

10μm

10μm

Fig. S8

a As prepared S in C matrix

C

S

S

e⁻

e⁻

e⁻

→ Li$_2$S$_{6,8}$ dissolution

b Heat-treated S in C

S

e⁻

e⁻

e⁻

e⁻

Electrolyte

Compact C layer serves as "molecular sieve"

Fig. S9